Ability of loss to increase the spatial coherence of guided waves

P. A. Brandão [*]
Instituto de Física, Universidade Federal de Alagoas, Maceió 57072-900, Brazil

(Received 30 May 2023; revised 24 July 2023; accepted 16 August 2023; published 25 August 2023)

When loss is introduced in one arm of a pair of coupled waveguides, it can result in an output signal with increased spatial coherence compared to the input beam. To theoretically investigate this phenomenon, we employ the formalism of classical coherence theory and develop a continuous model for the waveguides, treating them as a pair of Gaussian profiles. Our study focuses on the dynamics of the cross-spectral density function and the effective degree of coherence.

DOI: 10.1103/PhysRevA.108.023522

I. INTRODUCTION

In conventional optical experiments, it is typically assumed that any optical losses are undesirable due to their potential to introduce noise and degrade the accuracy of the measured signal. However, intentional induction of loss in a material has found applications in classical and quantum systems, such as loss-induced transparency [1], tunability of quantum interference [2,3], beam splitters [4], coherent perfect absorption [5], and verifications of true quantum parity-time ($\mathcal{PT}$)-symmetric systems [6], to cite a few. These discoveries are now part of a broader research field known as non-Hermitian optics [7–10], which originated from the pioneering work of Bender and Boettcher on the real spectra of non-Hermitian quantum $\mathcal{PT}$-symmetric potentials [11].

In 1998, Bender and Boettcher suggested that a class of nonrelativistic Hamiltonians having $\mathcal{PT}$ symmetry, although non-Hermitian with respect to the usual inner product, have a completely real spectrum [11,12]. This remarkable discovery has led to extensive research on potential generalizations of quantum theory [13,14]. Because there are several similarities between the formal mathematics of quantum mechanics and Maxwell's equations, non-Hermitian concepts have been integrated into optics, particularly in the refractive index of materials. For a one-dimensional (1D) quantum potential function to exhibit $\mathcal{PT}$ symmetry, the condition is that $V(x) = V^*(-x)$. In optics, a material is considered $\mathcal{PT}$ symmetric if its refractive index $n(x)$ satisfies the same condition. This implies that the real (imaginary) part of the refractive index is an even (odd) function of position. The first experimentally produced genuine $\mathcal{PT}$-symmetric material was a coupled system of waveguides that demonstrated a nonreciprocal light propagation [15].

With a few exceptions [16–24], most papers in the field of non-Hermitian optics assume the optical field to be fully coherent in both time and space. It has long been recognized that the primary factor governing field evolution is the fluctuation between distinct space-time points, which can be characterized by specific correlation functions [25–28]. These studies have demonstrated that gain and loss can affect the statistical properties of stochastic fields in scattering systems. In this paper, we consider the diffraction evolution inside materials possessing only loss, which are more easily created in laboratories. Our specific interest lies in exploring the potential to improve the control over the spatial coherence properties of a partially coherent beam that propagates through a coupled non-Hermitian waveguide system. The theory can be tested under experimental conditions using currently available photonic structures. [1].

Controlling the coherence of optical waves presents a significant challenge in the field of statistical optics. Several proposals have been published to address this issue, focusing on the generation of partially coherent beams in free space with adjustable coherence properties. These proposals include the superposition of Bessel beams [29], coherence with orbital angular momentum (OAM) [30], and the utilization of circularly coherent light [30], among others. The coherence properties of light have also been explored in the context of waveguides [31,32] and optical fibers [33,34]. However, previous studies predominantly considered the passive role of materials. In contrast, our theory bridges the gap between non-Hermitian optics and a specific aspect of classical coherence theory, namely the spatial coherence properties of guided waves. By unifying these concepts, we provide a different framework for understanding and manipulating the coherence of guided optical waves.

Section II discusses the physical model considered in the numerical calculations, as well as the coherence of the incident optical beam. Section III reviews the numerical method used to solve the evolution equation for the cross-spectral density. In Sec. IV, the principal findings are discussed by defining the effective degree of coherence to characterize spatial correlations. Finally, Sec. V presents the final remarks and conclusions.

II. WAVEGUIDE MODEL AND THE INCIDENT PARTIALLY COHERENT BEAM

In second-order classical coherence theory, assuming the scalar approximation, the fundamental correlation function in the space-time domain is the mutual coherence function,

[*]paulo.brandao@fis.ufal.br

defined as $\Gamma(\mathbf{r}_1, \mathbf{r}_2, \tau) = \langle u^*(\mathbf{r}_1, t)u(\mathbf{r}_2, t+\tau)\rangle$, which depends only on τ for a statistically stationary process (at least in the wide sense), and the average is performed over an ensemble of realizations of the field $u(\mathbf{r}, t)$ [25]. However, it is more desirable to work in the space-frequency domain with the cross-spectral density function $W(\mathbf{r}_1, \mathbf{r}_2, \omega)$, defined as the Fourier transform of the mutual coherence function, $W(\mathbf{r}_1, \mathbf{r}_2, \omega) = (1/2\pi)\int \Gamma(\mathbf{r}_1, \mathbf{r}_2, \tau)e^{i\omega\tau}\, d\tau$. It is also possible to interpret the cross-spectral density as the average of a suitable product of an ensemble of monochromatic components of the field [25].

In this context, we consider an optical beam $u(\mathbf{r}, t)$ that propagates mainly in the z direction with a transverse x-dependent field profile, where $\mathbf{r} = (x, z)$. It can be demonstrated that the cross-spectral density satisfies the partial differential equation

$$i\frac{\partial W_{12}}{\partial \xi} + \left(\frac{\partial^2}{\partial \eta_2^2} - \frac{\partial^2}{\partial \eta_1^2}\right)W_{12} + (V_2 - V_1^*)W_{12} = 0, \tag{1}$$

where $W_{12}(\xi) = W(\eta_1, \eta_2, \xi)$, $V_j = V(\eta_j)$, and the normalized coordinates (η, ξ) are given by $\eta = x/x_0$ and $\xi = z/2k_0 n_0 x_0^2$. Here, x_0 is an arbitrary scale factor, $k_0 = 2\pi/\lambda_0$, where λ_0 is the free-space wavelength. The potential function $V(\eta)$ is related to the refractive-index distribution $n(\eta) = n_0 + n_R(\eta) + in_I(\eta)$ by $V(\eta) = 2k_0^2 n_0 x_0^2[n_R(\eta) + in_I(\eta)]$ [35]. Here, n_0 is a real and positive number representing the background refractive index of the substrate, and n_j $(j = R, I)$ are real functions of position. The imaginary part is assumed to be positive to account for losses in the material. Once Eq. (1) is solved, the spectral density $S(\eta, \xi) = W(\eta, \eta, \xi)$ can be determined, which represents the average beam intensity at distance ξ from the initial plane.

There are various ways to model a coupled system of waveguides. We have opted for the simplest approach, which involves using continuous Gaussian functions. This enables us to observe the effects without sacrificing generality. To accomplish this, we consider the double Gaussian model for two coupled waveguides, defined as

$$V(\eta) = V_0 e^{-(\eta/w)^2} + (V_0 + i\beta)e^{-(\eta-d)^2/w^2}. \tag{2}$$

The parameter V_0 regulates the real part of the waveguide's refractive index, while the non-Hermitian parameter β controls the loss rate of the waveguide centered at $\eta = d$. Additionally, the waveguide width is characterized by the parameter w. A plot of the potential model is shown in Fig. 1. The model represented by Eq. (2) has the advantage of being well behaved so that it generates less numerical error in the spectral method used, as described below.

To model the incident partially coherent beam, we have selected the Gaussian-Schell model, which has been thoroughly examined in laboratories, and its properties are widely understood [36]. Suppose that at the entrance of WG_1, the spectral density $S(\eta, 0)$ and the spectral degree of coherence $\mu(\eta_1, \eta_2, 0)$ are given by

$$S(\eta, 0) = e^{-\eta^2/2\sigma_I^2}, \tag{3}$$

$$\mu(\eta_1, \eta_2, 0) = e^{-(\eta_1-\eta_2)^2/2\sigma_\mu^2}, \tag{4}$$

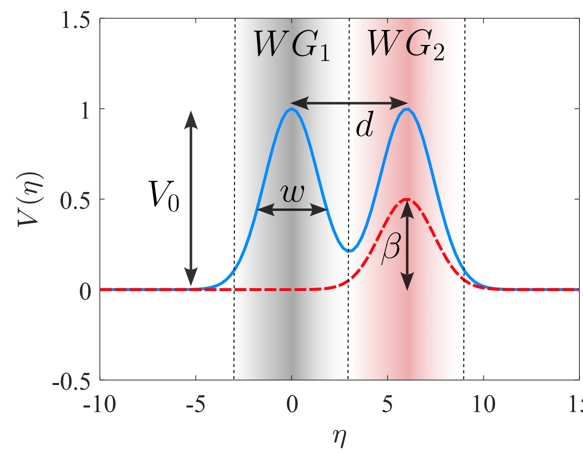

FIG. 1. Plot of the potential function (2) for $V_0 = 1$, $w = 2$, $d = 6$, and $\beta = 1/2$. The blue continuous line represents the real part, while the red dashed line represents the imaginary part of $V(\eta)$.

where σ_I and σ_μ represent the beam width and the spatial coherence parameter, respectively. In the limit $\sigma_\mu \to \infty$, the fully coherent Gaussian beam is recovered. The incident cross-spectral density is given by $W(\eta_1, \eta_2, 0) = [S(\eta_1, 0)S(\eta_2, 0)]^{1/2}\mu(\eta_1, \eta_2, 0)$. The main objective of this paper is to investigate the changes in spatial coherence properties, specifically defined by the effective spectral degree of coherence (Sec. IV), as the guided wave propagates.

III. NUMERICAL METHOD

Equation (1) can be solved by using standard split-step Fourier transform techniques [37]. Since this method is usually applied in 1D and 2D paraxial wave equations, we highlight here the main differences that occur in dealing with Eq. (1). To start, write the evolution equation as $\partial W_{12}(\xi)/\partial\xi = i(\nabla_{12}^2 + \mathcal{V})W_{12}(\xi)$, where $\nabla_{12}^2 = \partial^2/\partial\eta_2^2 - \partial^2/\partial\eta_1^2$ and $\mathcal{V} = V_2 - V_1^*$. The formal solution to this equation is given by

$$W_{12}(\xi) = e^{i(\nabla_{12}^2 + \mathcal{V})\xi}W_{12}(0). \tag{5}$$

Equation (5) can be used to obtain the new values of the cross-spectral density after step $\Delta\xi$: $W_{12}(\xi + \Delta\xi) = e^{i(\nabla_{12}^2 + \mathcal{V})\Delta\xi}W_{12}(\xi)$. To implement this algorithm, we employ the approximation

$$e^{i\Delta\xi(\nabla_{12}^2 + \mathcal{V})} \approx e^{i\mathcal{V}\Delta\xi/2}e^{i\Delta\xi\nabla_{12}^2}e^{i\mathcal{V}\Delta\xi/2}, \tag{6}$$

introducing an error $O(\Delta\xi^3)$ after each step [38]. The first exponential acting on $W_{12}(0)$ can be performed by a simple matrix multiplication. Then, the second exponential factor involving the operator ∇_{12}^2 can be applied by using the Fourier transform,

$$e^{i\Delta\xi\nabla_{12}^2}g_{12}(\xi) = \mathcal{F}_{12}^{-1}\{e^{i\Delta\xi(k_1^2 - k_2^2)}\mathcal{F}_{12}\{g_{12}(\xi)\}\}, \tag{7}$$

where (k_1, k_2) are the Fourier spatial frequencies and $\mathcal{F}_{12}$ denotes a two-dimensional Fourier transform operation having an inverse $\mathcal{F}_{12}^{-1}$.

The presence of a minus sign in the free-space propagator $e^{i\Delta\xi(k_1^2 - k_2^2)}$ for the cross-spectral density implies that $W(\eta_1, \eta_2, \xi)$ evolves under a different dynamics when

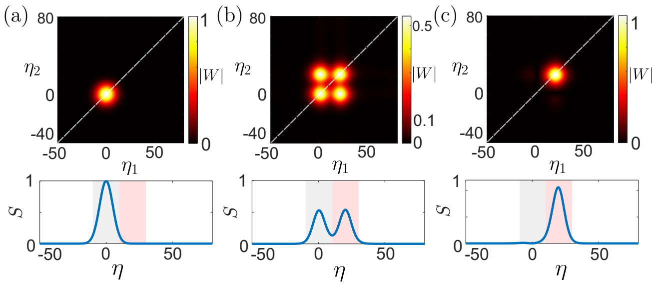

FIG. 2. The cross-spectral density $W(\eta_1, \eta_2, \xi)$ evolves in the presence of lossless waveguides with $\beta = 0$ and under high coherence conditions, where $\sigma_\mu = 40$ and $\sigma_I = 5$. The top row displays three snapshots of $|W(\eta_1, \eta_2, \xi)|$ at (a) $\xi = 0$, (b) $\xi = 135$, and (c) $\xi = 270$, capturing a complete energy transfer between the waveguides. The dashed diagonal line corresponds to values of the spectral density $S(\eta, \xi) = W(\eta, \eta, \xi)$, shown below each corresponding plot. The parameters utilized are as follows: $V_0 = 0.1$, $w = 10$, and $d = 20$.

compared to the free-space evolution of a coherent two-dimensional optical beam $E(x, y, z)$ [20]. In all simulations, we used a computational window of size $L \times L$ with $L = 300$, having 2^{10} points in each direction, and the fast Fourier transform algorithm was used to calculate Eq. (7).

IV. DYNAMICS OF THE EFFECTIVE DEGREE OF COHERENCE

To characterize the spatial coherence of the optical beam inside the waveguides, we use the effective degree of coherence μ, defined as [39–41]

$$\mu^2(\xi) = \frac{\iint_{A^2} |W(\eta_1, \eta_2, \xi)|^2 \, d\eta_1 d\eta_2}{\left[\int_A S(\eta, \xi) d\eta\right]^2}, \tag{8}$$

where $A^2 = [-d/2, 3d/2] \cup [-d/2, 3d/2]$ is the total transverse waveguide "area" (the dashed lines $\eta = -d/2$, $\eta = d/2$, and $\eta = 3d/2$ are shown in Fig. 1). Values of this parameter such that $\mu = 1$ imply a high coherence and are bounded below by zero (implying a lack of spatial coherence). Definition (8) can also be viewed as the rms average of the two-point spectral degree of coherence weighted by the spectral density in A [41]. This definition is convenient as it considers the intensities of the field in a finite region. Additionally, it is more suitable for numerical implementation. With this in place, we are now prepared to explore the dynamics of the spectral degree of coherence in both passive and lossy waveguide systems.

A. Lossless waveguide

Consider a passive waveguide with $\beta = 0$. Figure 2 displays three snapshots of the cross-spectral density for different values of ξ during a complete transfer of optical energy between the two waveguides. We chose $\sigma_\mu = 40$ and $\sigma_I = 5$ to generate a spatially coherent propagation. The transverse profile of the spectral density is also shown below each plot, representing a diagonal cross-sectional cut of $W_{12}(\xi)$.

The appearance of four lobes in (η_1, η_2) space at $\xi = 135$ can be explained more clearly by a discrete version of field propagation. If $E_n(\xi)$ is the field amplitude at waveguide n ($\xi_n = nd$), then $idE_n(\xi)/d\xi + \gamma E_n(\xi) + C[E_{n-1}(\xi) + E_{n+1}(\xi)] = 0$, where γ is the propagation constant, which is the same for each waveguide, and C is the coupling constant. The discrete version $W_{nm}(\xi)$ of the cross-spectral density thus satisfies $idW_{n,m}/d\xi = C(W_{n+1,m} + W_{n-1,m} - W_{n,m+1} - W_{n,m-1})$ and in the special case involving two waveguides $n = 1$ and 2, we have $dS_1/d\xi = -2C\,\mathrm{Im}(W_{12})$, $dS_2/d\xi = 2C\,\mathrm{Im}(W_{12})$, and $idW_{12}/d\xi = C(S_2 - S_1)$, where $W_{11} = S_1$ and $W_{22} = S_2$ are the spectral densities in waveguides 1 and 2, respectively. Thus, there are four sites excited in the (η_1, η_2) plane during propagation in this discrete version, $W_{11} = S_1$, $W_{12} = W_{21}^*$, and $W_{22} = S_2$ which explains the observed pattern in Fig. 2. A comprehensive theory of discrete spatial coherence in waveguide arrays is currently under investigation and will be published elsewhere. The subsequent discussion exclusively concerns continuous functions. Note that in this lossless scenario the propagation constants are the same for both waveguides.

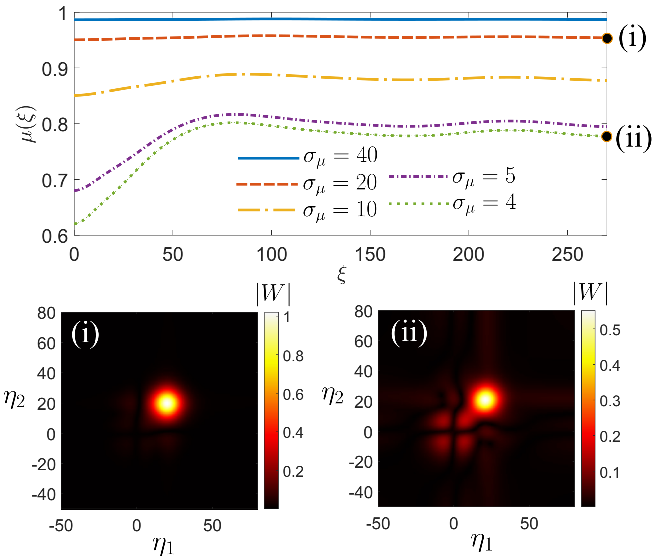

FIG. 3. Dynamics of the effective degree of coherence in lossless waveguides. Evolution $\mu(\xi)$, calculated from Eq. (8), for several values of σ_μ. Two snapshots of $|W(\eta_1, \eta_2, \xi)|$ are shown for (i) and (iii) marked in the plot. The other parameters are the same as in Fig. 2.

The dynamics depicted in Fig. 2 exhibit remarkable coherence, as indicated by the constant value of $\mu \approx 1$ throughout the entire range of propagated distance (further discussed below). Before delving into a comparison with dissipative dynamics, it is also of interest to investigate the behavior of guided waves with low spatial coherence in this lossless scenario.

Figure 3 displays plots of $\mu(\xi)$, calculated from Eq. (8), for five values of the coherence parameter $\sigma_\mu = 40$, 20, 10, 5, and 4, while keeping the incident beam width fixed at $\sigma_I = 5$. The largest value ($\sigma_\mu = 40$), represented by the continuous blue line, is the same as used in Fig. 2. It can be observed that the beam remains spatially coherent throughout the exchange of optical energy between the waveguides. A similar behavior is observed for $\sigma_\mu = 20$ (dashed orange line) and $\sigma_\mu = 10$ (long dashed-dotted yellow line). However, for lower values, such as

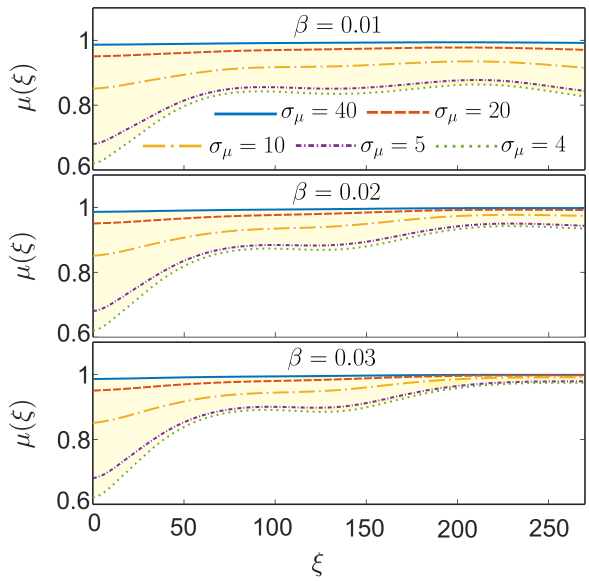

FIG. 4. Effective degree of coherence [Eq. (8)] as a function of propagation distance ξ for dissipative waveguides. Each continuous line represents one value of σ_μ exactly as in Fig. 3. The graph displays three plots representing increasing values of the loss parameter $\beta = 0.01$, 0.02, and 0.03. The remaining parameters are the same as in Fig. 3.

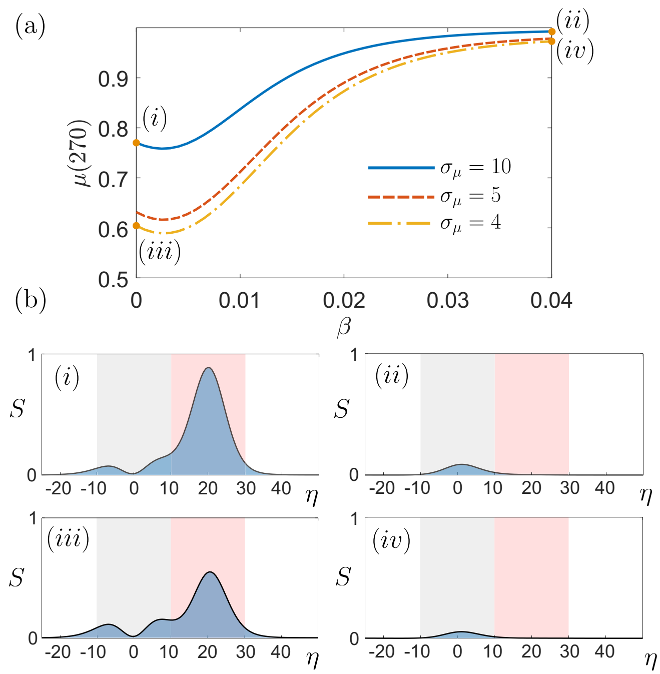

FIG. 5. (a) Effective degree of coherence at $\xi = 270$ as a function of the loss parameter β for three values of $\sigma_\mu = 10$, 5, and 4. (b) Spectral density profiles S for the points marked (i), (ii), (iii), and (iv).

$\sigma_\mu = 5$ (short dashed-dotted purple line) and $\sigma_\mu = 4$ (dotted green line), the effective degree of coherence increases as the beam propagates. They reach a maximum value of $\mu \approx 0.8$ around $\xi \approx 60$ and remain approximately stable thereafter.

To confirm that the statistical correlations between field amplitudes are significantly influenced in this low coherence regime (by the field itself and the geometry considered), two snapshots of $|W_{12}(\xi)|$ at $\xi = 270$ are shown for $\sigma_\mu = 20$ and $\sigma_\mu = 4$. The reader can infer the spectral density by inspecting these plots in the same way as we did in Fig. 2. Notice that these complex pattern deformations of the cross-spectral density cannot be captured by the simple discrete model introduced earlier.

The evolution of the spectral density in the low coherence regime closely resembles the high coherence case, with the exception that at $\xi = 0$, there is a slight energy leakage caused by the inefficient coupling of a partially coherent beam to the waveguide WG_1. This is due to the fact that a partially coherent beam tends to spread more during propagation compared to a fully coherent beam. However, after an initial transient leaking, the partially coherent wave remains confined within the waveguide system.

These results indicate that a passive waveguide system has the potential to enhance the spatial coherence among the guided waves (for the considered parameters and geometry). We will now examine the impact of introducing loss to one of the waveguides and investigate how energy dissipation influences the behavior of the effective degree of coherence.

B. Lossy waveguide

Figure 4 shows the evolution of the effective degree of coherence $\mu(\xi)$ in the case where WG_2 dissipates energy at rate β. All parameters are the same as in Fig. 2, except that $\beta \neq 0$. Remarkably, these curves suggest that as β increases, an initially spatially incoherent beam can gain coherence during propagation. The yellow shaded area marks the boundary between minimum and maximum values of $\mu(\xi)$. To confirm that indeed the effective degree of coherence increases, we fix $\xi = 270$ and inspect what happens to μ as a function of β. Figure 5(a) reveals that, beyond a minimum value of $\beta \approx 0.005$, the optical beam becomes more spatially coherent as the amount of loss into WG_2 increases. Of course, this is accompanied by a decrease of optical intensities, as revealed in Fig. 5(b). It must be remarked that the standard definition of the spectral degree of coherence as a two-point correlation function also reveals an increase of the spatial coherence between the waveguides as β increases.

It should be noted that as the loss rate β reaches a sufficiently high value, Rabi-like oscillations between the waveguides cease to occur. In this scenario, the incident optical beam remains confined to the passive waveguide. Interestingly, the energy transmission throughout the entire structure actually increases with increasing β. This phenomenon is known as loss-induced transparency [1]. The corresponding behavior is evident in the plots of the spectral density shown in Fig. 5(b). For $\beta = 0.04$, it can be observed that the optical beam at (ii) and (iv) is localized around WG_1, and Rabi-like oscillations no longer occur as in cases (i) and (iii). By carefully incorporating lossy factors into the structure, we anticipate nontrivial changes in the effective degree of coherence.

To explain this effect, one must examine the correlation distribution amplitude of the cross-spectral density W_{12} in the (η_1, η_2) plane. The reason why μ increases in the lossless case

(Fig. 3) is because the spectral density S decreases slightly faster over the region A during propagation compared to the region A^2 occupied by W_{12}. This discrepancy arises from the fact that the field energy present in the line $\eta_1 = \eta_2$ spreads out in the (η_1, η_2) plane right from the beginning of the propagation. When loss is introduced, this effect is amplified, leading to a more rapid decrease in the spectral density compared to W_{12}. Consequently, the fraction in Eq. (8) increases. Thus, a strategy to design systems that enhance spatial coherence involves the careful engineering of non-Hermitian profiles $V(\eta)$ in a way that promotes a faster decrease in the field energy $S(\eta, \xi)$ compared to $W(\eta_1, \eta_2, \xi)$ over the same region.

One possible method to experimentally confirm the findings presented in this study is to generate a Gaussian-Schell optical beam using a rotating diffuser [36] and then focus the transmitted beam at the entrance of WG_1. Subsequently, the output signals at WG_1 and WG_2 can be directed towards a double-slit setup, allowing the measurement of fringe visibility. This measurement provides direct information about the spectral degree of coherence. Thus, an increase in visibility should be observed as the level of loss in one of the waveguide arms increases. It is worth noting that the loss mechanism related to the parameter β does not necessarily have to involve a material located inside the waveguide. Instead, it can be achieved by coupling smaller waveguides to WG_2 in order to enable the leakage of optical energy.

V. CONCLUSIONS

These observations prompt an intriguing question: Can we develop a "coherence management" system analogous to diffraction management [42] to engineer structures that generate desired coherence properties? It should function as a type of coherence filter, giving output fields that are highly correlated over some waveguides and highly uncorrelated at others. Something similar has been proposed for speckle beams [43]. Currently, to the best of my knowledge, the answers to these questions remain unknown.

In conclusion, waveguide arrays offer a versatile approach to customizing the coherence characteristics of optical beams. By introducing loss into the system, we can observe intricate alterations in the spectral degree of coherence, which hold potential for integrated optics applications. However, there is still much research to be conducted in order to gain a deeper understanding of how dissipative systems influence the coherence properties of classical waves. Our findings may represent an initial step in this direction, paving the way for further investigations in this field.

ACKNOWLEDGMENTS

We wish to acknowledge the financial support of CNPq (Conselho Nacional de Desenvolvimento Científico e Tecnológico) and FAPEAL (Fundação de Amparo à Pesquisa do Estado de Alagoas).

[1] A. Guo, G. J. Salamo, D. Duchesne, R. Morandotti, M. Volatier-Ravat, V. Aimez, G. A. Siviloglou, and D. N. Christodoulides, Observation of $\mathcal{PT}$-Symmetry Breaking in Complex Optical Potentials, Phys. Rev. Lett. **103**, 093902 (2009).

[2] R. Uppu, T. A. Wolterink, T. B. Tentrup, and P. W. Pinkse, Quantum optics of lossy asymmetric beam splitters, Opt. Express **24**, 16440 (2016).

[3] B. Vest, M.-C. Dheur, É. Devaux, A. Baron, E. Rousseau, J.-P. Hugonin, J.-J. Greffet, G. Messin, and F. Marquier, Anti-coalescence of bosons on a lossy beam splitter, Science **356**, 1373 (2017).

[4] S. M. Barnett, J. Jeffers, A. Gatti, and R. Loudon, Quantum optics of lossy beam splitters, Phys. Rev. A **57**, 2134 (1998).

[5] T. Roger, S. Vezzoli, E. Bolduc, J. Valente, J. J. Heitz, J. Jeffers, C. Soci, J. Leach, C. Couteau, N. I. Zheludev *et al.*, Coherent perfect absorption in deeply subwavelength films in the single-photon regime, Nat. Commun. **6**, 7031 (2015).

[6] F. Klauck, L. Teuber, M. Ornigotti, M. Heinrich, S. Scheel, and A. Szameit, Observation of pt-symmetric quantum interference, Nat. Photonics **13**, 883 (2019).

[7] S. Longhi, Parity-time symmetry meets photonics: A new twist in non-Hermitian optics, Europhys. Lett. **120**, 64001 (2017).

[8] H. Zhao and L. Feng, Parity–time symmetric photonics, Natl. Sci. Rev. **5**, 183 (2018).

[9] S. K. Gupta, Y. Zou, X.-Y. Zhu, M.-H. Lu, L.-J. Zhang, X.-P. Liu, and Y.-F. Chen, Parity-time symmetry in non-Hermitian complex optical media, Adv. Mater. **32**, 1903639 (2020).

[10] T. Kottos, Broken symmetry makes light work, Nat. Phys. **6**, 166 (2010).

[11] C. M. Bender and S. Boettcher, Real Spectra in Non-Hermitian Hamiltonians Having $\mathcal{PT}$ Symmetry, Phys. Rev. Lett. **80**, 5243 (1998).

[12] C. M. Bender, Making sense of non-Hermitian Hamiltonians, Rep. Prog. Phys. **70**, 947 (2007).

[13] C. M. Bender, D. C. Brody, and H. F. Jones, Complex Extension of Quantum Mechanics, Phys. Rev. Lett. **89**, 270401 (2002).

[14] A. Mostafazadeh, Pseudo-Hermiticity versus PT symmetry: The necessary condition for the reality of the spectrum of a non-Hermitian Hamiltonian, J. Math. Phys. **43**, 205 (2002).

[15] C. E. Rüter, K. G. Makris, R. El-Ganainy, D. N. Christodoulides, M. Segev, and D. Kip, Observation of parity–time symmetry in optics, Nat. Phys. **6**, 192 (2010).

[16] P. A. Brandão and S. Cavalcanti, Non-Hermitian spectral changes in the scattering of partially coherent radiation by periodic structures, Opt. Lett. **44**, 4363 (2019).

[17] P. A. Brandão and S. B. Cavalcanti, Scattering of partially coherent radiation by non-Hermitian localized structures having parity-time symmetry, Phys. Rev. A **100**, 043822 (2019).

[18] P. A. Brandão, J. P. Mendonça, and S. Cavalcanti, Low coherence-induced resonance in double-layer structures having parity–time symmetry, Opt. Lett. **46**, 717 (2021).

[19] P. A. Brandão and O. Korotkova, Scattering theory for stationary materials with $\mathcal{PT}$ symmetry, Phys. Rev. A **103**, 013502 (2021).

[20] P. A. Brandão and J. C. A. Rocha, Propagation of partially coherent light in non-Hermitian lattices, Phys. Rev. A **106**, 063503 (2022).
[21] O. Korotkova and P. A. Brandão, Light scattering from stationary $\mathcal{PT}$-symmetric collections of particles, Opt. Lett. **46**, 1417 (2021).
[22] D. G. Pires, N. M. Litchinitser, and P. A. Brandão, Scattering of partially coherent vortex beams by a $\mathcal{PT}$-symmetric dipole, Opt. Express **29**, 15576 (2021).
[23] X. Zhang, Y. Liu, Y. Chen, F. Wang, and Y. Cai, Noncentrosymmetric far-zone spectral density induced by light scattering with random media having parity-time symmetry, Phys. Rev. A **105**, 023510 (2022).
[24] X. Zhang, Y. Chen, F. Wang, and Y. Cai, Scattering of partially coherent vector beams by a deterministic medium having parity-time symmetry, Photonics **9**, 140 (2022).
[25] E. Wolf, *Introduction to the Theory of Coherence and Polarization of Light* (Cambridge University Press, Cambridge, U.K., 2007).
[26] L. Mandel and E. Wolf, *Optical Coherence and Quantum Optics* (Cambridge University Press, Cambridge, U.K., 1995).
[27] O. Korotkova, *Random Light Beams: Theory and Applications* (CRC Press, Boca Raton, FL, 2017).
[28] O. Korotkova and G. Gbur, Applications of optical coherence theory, Prog. Opt. **65**, 43 (2020).
[29] M. A. Pinto and P. A. Brandão, Frozen spatial coherence, Opt. Lett. **47**, 3055 (2022).
[30] O. Korotkova, S. Pokharel, and G. Gbur, Tailoring the coherence–OAM matrices, Opt. Lett. **47**, 6109 (2022).
[31] S. Abdullaev, Spatial coherence of the optical field in multimode waveguides, Sov. J. Quantum Electron. **14**, 613 (1984).
[32] I. Deryugin, S. Abdullaev, and A. T. Mirzaev, Coherence of the electromagnetic field in dielectric waveguides, Sov. J. Quantum Electron. **7**, 1243 (1977).
[33] A. Efimov, Spatial coherence at the output of multimode optical fibers, Opt. Express **22**, 15577 (2014).
[34] A. Efimov, Different measures of speckle and coherence at the output of a multimode optical fiber, J. Opt. Soc. Am. A **36**, 1 (2019).
[35] K. G. Makris, R. El-Ganainy, D. N. Christodoulides, and Z. H. Musslimani, Beam Dynamics in $\mathcal{PT}$ Symmetric Optical Lattices, Phys. Rev. Lett. **100**, 103904 (2008).
[36] Q. He, J. Turunen, and A. T. Friberg, Propagation and imaging experiments with Gaussian Schell-model beams, Opt. Commun. **67**, 245 (1988).
[37] M. R. Hermann and J. A. Fleck, Jr., Split-operator spectral method for solving the time-dependent Schrödinger equation in spherical coordinates, Phys. Rev. A **38**, 6000 (1988).
[38] J. Javanainen and J. Ruostekoski, Symbolic calculation in development of algorithms: Split-step methods for the Gross–Pitaevskii equation, J. Phys. A: Math. Gen. **39**, L179 (2006).
[39] K. Blomstedt, T. Setälä, and A. T. Friberg, Effective degree of coherence: A second look, J. Opt. Soc. Am. A **32**, 718 (2015).
[40] K. Blomstedt, T. Setälä, and A. T. Friberg, Effective degree of coherence: General theory and application to electromagnetic fields, J. Opt. A: Pure Appl. Opt. **9**, 907 (2007).
[41] P. Vahimaa and J. Tervo, Unified measures for optical fields: Degree of polarization and effective degree of coherence, J. Opt. A: Pure Appl. Opt. **6**, S41 (2004).
[42] H. S. Eisenberg, Y. Silberberg, R. Morandotti, and J. S. Aitchison, Diffraction Management, Phys. Rev. Lett. **85**, 1863 (2000).
[43] R. Ma, H. H. Zhang, E. Manuylovich, S. Sugavanam, H. Wu, W. L. Zhang, V. Dvoyrin, T. P. Hu, Z. J. Hu, Y. J. Rao *et al.*, Tailoring of spatial coherence in a multimode fiber by selectively exciting groups of eigenmodes, Opt. Express **28**, 20587 (2020).